Modelling tree-ring cellulose $\delta^{18}O$ variations of two temperature-sensitive tree species from North and South America

Authors:

Aliénor Lavergne[1], Fabio Gennaretti[1], Camille Risi[2], Valérie Daux[3], Etienne Boucher[4], Martine M. Savard[5], Maud Naulier[6], Ricardo Villalba[7], Christian Bégin[5] and Joël Guiot[1]

[1]Aix Marseille Université, CNRS, IRD, Collège de France, CEREGE, ECCOREV, Aix-en-Provence, France

[2]Laboratoirede Météorologie Dynamique, IPSL, UPMC, CNRS, Paris, France

[3]Laboratoire des Sciences du Climat et de l'Environnement, CEA-CNRS-UVSQ, 91191 Gif-sur-Yvette, France

[4]Department of Geography and GEOTOP, Université du Québec à Montréal, Montréal, Canada

[5]Geological Survey of Canada, Natural Resources Canada, 490 rue de la Couronne, QC, G1K9A9, Canada

[6]Institut de Radioprotection et de Sureté Nucléaire (IRSN), PRP-ENV, SERIS/LRTE, Saint-Paul-lez-Durance, France

[7]Instituto Argentino de Nivología, Glaciología y Ciencias Ambientales, IANIGLA-CONICET, Mendoza, Argentina

Corresponding authors: Aliénor Lavergne (alienor.lavergne@gmail.com) and Fabio Gennaretti (gennaretti@cerege.fr)

Tel : +33 (0) 4 42 97 15 32

Centre Européen de Recherche et d'Enseignement en Géosciences

Technopôle de l'Arbois-Méditerranée

13545 Aix-en-Provence, FRANCE

ABSTRACT

Oxygen isotopes in tree rings ($\delta^{18}O_{TR}$) are widely used to reconstruct past climates. However, the complexity of climatic and biological processes controlling isotopic fractionation is not yet fully understood. Here, we use the MAIDENiso model to decipher the variability of $\delta^{18}O_{TR}$ of two temperature-sensitive species of relevant paleoclimatological interest (*Picea mariana* and *Nothofagus pumilio*) and growing at cold high-latitudes in North and South America. In this first modelling study on $\delta^{18}O_{TR}$ values in both northeastern Canada (53.86°N) and western Argentina (41.10°S), we specifically aim at: 1) evaluating the predictive skill of MAIDENiso to simulate $\delta^{18}O_{TR}$ values, 2) identifying the physical processes controlling $\delta^{18}O_{TR}$ by mechanistic modelling and, 3) defining the origin of the temperature signal recorded in the two species. Although the linear regression models used here to predict daily $\delta^{18}O$ of precipitation ($\delta^{18}O_P$) may need to be improved in the future, the resulting daily $\delta^{18}O_P$ values adequately reproduce observed (from weather stations) and simulated (by global circulation model) $\delta^{18}O_P$ series. The $\delta^{18}O_{TR}$ values of the two species are correctly simulated using the $\delta^{18}O_P$ estimation as MAIDENiso input, although some offset in mean $\delta^{18}O_{TR}$ levels is observed for the South American site. For both species, the variability of $\delta^{18}O_{TR}$ series is more likely linked to the effect of temperature on isotopic enrichment of the leaf water rather than on the isotopic composition of the source water. We show that MAIDENiso is a powerful tool for investigating isotopic fractionation processes but that the lack of a denser isotope-enabled monitoring network recording oxygen fractionation in the soil-vegetation-atmosphere compartments limits our capacity to decipher the processes at play. This study proves that the eco-physiological modelling of $\delta^{18}O_{TR}$ values is necessary to interpret the recorded climate signal more reliably.

Keywords: MAIDENiso model, $\delta^{18}O$, tree-ring, *Nothofagus pumilio*, *Picea mariana*

1. INTRODUCTION

Oxygen isotopes in tree rings ($\delta^{18}O_{TR}$) are increasingly used as indicators of past climatic changes in temperate areas (Cernusak and English, 2015; Hartl-Meier et al., 2014; Saurer et al., 2008). They have been widely used to reconstruct past atmospheric conditions such as air temperature (Naulier et al., 2015), drought (Labuhn et al., 2016), precipitation amount (Rinne et al., 2013), isotopic composition of precipitation (Danis et al., 2006), relative air humidity (Wernicke et al., 2015), cloud cover (Shi et al., 2012), and even atmospheric circulation patterns (Brienen et al., 2012). This diversity of climatic targets possibly reconstructed based on oxygen isotopes hints at the challenge of understanding the complexity of the climatic and biological processes that control isotopic fractionation of oxygen in trees (Treydte et al., 2014). Uncertainties arise because different poorly measured factors influence $\delta^{18}O_{TR}$ values. Isotopic signals in tree-rings cellulose are strongly influenced by isotopic signature of soil water taken up by the roots and by evaporative and physiological processes occurring at the leaf level and during downstream metabolism (Barbour et al., 2005; Gessler et al., 2014). Thus, a comprehensive approach that embraces existing mechanistic understanding of the fractionation processes involved is required.

Few isotopic process-based models have been developed to investigate the mechanistic rules governing the $\delta^{18}O_{TR}$ variations (Guiot et al., 2014): the Péclet-modified Craig-Gordon model (Kahmen et al., 2011) and the Roden's model (Roden et al., 2000) are able to estimate, at a daily time step, the $\delta^{18}O$ values of soil and xylem waters, and the isotopic fractionation occurring in the leaves due to evapotranspiration. Versions of these models are integrated in more complete forest ecophysiological models simulating the ensemble of forest water and carbon fluxes: (1) MAIDEN (Modeling and Analysis In DENdroecology) (Gea-Izquierdo et al., 2015; Misson, 2004), which contains the isotopic module MAIDENiso (Danis et al., 2012) and (2) MUSICA (Ogée et al., 2003, 2009). Both are accounting for important post-photosynthetic factors and are able to link photosynthesis and carbohydrate allocation to stem growth.

In this paper, we use the MAIDENiso model to decipher the $\delta^{18}O_{TR}$ variability in American temperature-sensitive species (*Picea mariana* in northeastern Canada and *Nothofagus pumilio* in western Argentina). The selected sites are of special interest for paleoclimatology given that their

$\delta^{18}O_{TR}$ chronologies carry strong temperature signals. A summer temperature reconstruction was already developed at the North American site (Gennaretti et al., 2017b; Naulier et al., 2015) and a calibration study conducted at the South American one highlighted the strong potential of $\delta^{18}O_{TR}$ values to reflect variations in summer-autumn temperatures over a large region south of 38°S (Lavergne et al., 2016). However, up to now, the climate-$\delta^{18}O_{TR}$ relationships were analysed using a black box approach based on linear models. Here, we specifically aim at: 1) evaluating the predictive skill of MAIDENiso to simulate $\delta^{18}O_{TR}$ values, 2) identifying the physical processes controlling $\delta^{18}O_{TR}$ by mechanistic modelling and, 3) defining the origin of the temperature signal recorded in the two species.

2. DATA AND METHODS

2.1. Sampling sites and tree-ring data

Two high-latitude American native species were studied here: 1) *Picea mariana* (Mill. B.S.P.; black spruce), which is a conifer widely distributed over the American boreal forest (Viereck and Johnston, 1990); and 2) *Nothofagus pumilio* (Poepp. et Endl. Krasser; lenga), which is an angiosperm deciduous species dominating the high-elevation forests along the Patagonian Andes from 35°S to 55°S (Donoso, 1981; Schlatter, 1994). We selected two sites of *P. mariana* in the centre of the Quebec-Labrador Peninsula in northeastern Canada (L01 and L20; from 53°51'N-72°24'W to 54°33'N-71°14'W, ~480 m elevation; see Gennaretti et al. (2014) and Naulier et al. (2014) for details) and three sites of *N. pumilio* in northern Patagonia, western Argentina (NUB, ALM and CHA; from 41°09′S-71°48′W to 41°15′S-71°17′W, 1270-1610 m elevation; see Lavergne et al. (2016, 2017) for details). Climate in northeastern Canada is mostly continental and subarctic with short, mild and wet summers and long, cold and dry winter. Total annual precipitation averages 825 mm with up to 46% falling during the growing season in summer (June to September) (Naulier et al., 2014). In western Argentina, precipitation is largely concentrated from late fall to early spring (May-November) followed by a drier and mild period during summer and early fall (December-April) (López Bernal et al., 2012).

Four trees per site were collected for both species. The selection of the samples and analytical procedure for $\delta^{18}O_{TR}$ measurements were described in Lavergne et al. (2016) and Naulier et al.

(2014). The developed $\delta^{18}O_{TR}$ chronologies covered the 1950-2005 and 1952-2011 periods at the northeastern Canadian and western Argentinian sites, respectively. The chronologies that were built for each species were significantly correlated between stands (Figure 1). This supported the construction of a combined isotope chronology for both the northeastern Canada and western Argentina sites.

2.2. Modelling oxygen isotopes in tree-ring cellulose with MAIDENiso

MAIDENiso is a process-based model that can simulate in parallel phenological and meteorological controls on photosynthetic activity and carbon allocation (Danis et al., 2012). It explicitly allocates carbohydrates to different carbon pools (leaves, stem, storage and roots) on a daily basis using phenological stage-dependent rules (see Gennaretti et al. (2017b) for details on the construction of the main MAIDEN model). It also simulates the fractionation of carbon and oxygen isotopes during growth processes. In particular, it estimates at a daily time step $\delta^{18}O$ values of soil water and xylem water, the isotopic fractionation occurring in the leaves due to evapotranspiration and the biochemical fractionation during cellulose formation. It uses as input daily maximum and minimum temperature (°C), precipitation (cm/day), atmospheric CO_2 concentration (ppm) and $\delta^{18}O$ values of precipitation ($\delta^{18}O_P$ in ‰). The code of the model can be found here: https://doi.org/10.6084/m9.figshare.5446435.v1.

In this study, the calculation of the daily $\delta^{18}O_{TR}$ in tree-ring cellulose (‰) is based on the (Danis et al., 2012)'s formulation of the Craig-Gordon model (Craig and Gordon, 1965):

$$\delta^{18}O_{TR} = (1-f_o)\cdot[\varepsilon^* + \varepsilon_k \cdot(1-h_{air}) + h_{air}\cdot\delta^{18}O_V + (1-h_{air})\cdot\delta^{18}O_{XW}] + f_o \cdot \delta^{18}O_{XW} + \varepsilon_0 \quad (1)$$

This equation summarizes how $\delta^{18}O_{TR}$ is determined by:

(i) the $\delta^{18}O$ of the source (xylem) water ($\delta^{18}O_{XW}$), which is computed by averaging the $\delta^{18}O_{SW}$ values of the different soil layers weighted by the volume of water taken up by the roots in each layer. The isotopic effects of water mixing and soil evaporation on the $\delta^{18}O_{SW}$ values of the different soil layers are computed by a mass and isotopic balance (Danis et al., 2012). It is worth noting that no fractionation occurs during water uptake by roots (Wershaw et al., 1966), neither during the transport of water from the roots to the leaves.

(ii) the ^{18}O enrichment of the leaf water due to transpiration is described by $(\varepsilon^{*}+\varepsilon_k\cdot(1-h_{air})+h_{air}\cdot\delta^{18}O_V+(1-h_{air})\cdot\delta^{18}O_{XW})$ after (Craig and Gordon, 1965), where:

a. ε^{*} is the equilibrium fractionation due to the change of phase from liquid water to vapour at the leaf temperature (fixed at 21.4°C, the temperature threshold for maximum carbon assimilation, ε^{*} is 9.65‰ (Helliker and Richter, 2008)),

b. ε_k is the kinetic fractionation due to the diffusion of vapour into unsaturated air through the stomata and the leaf boundary layer,

c. h_{air} is the relative humidity of the evaporating air mass estimated from daily air temperature (T_{air}; °C; mean of the maximum and minimum air temperatures), and the dew point temperature (T_r; °C) (Running et al., 1987),

d. $\delta^{18}O_V$ is the atmospheric water vapour calculated assuming a precipitation-vapour isotopic equilibrium (see below);

(iii) the biochemical fractionations (ε_0) due to oxygen exchange between carbonyl groups (C = O) in the organic molecules and water (DeNiro and Epstein, 1979; Farquhar et al., 1998).

(iv) the dampening factor f_o reflecting the exchange of the oxygen atoms between sucrose and xylem water during cellulose synthesis in the xylem cells of tree rings.

As previously evoked (i), $\delta^{18}O_{XW}$ of Eq. 1 depends on $\delta^{18}O_{SW}$ and thus on $\delta^{18}O_P$ values. However, long continuous time series of $\delta^{18}O_P$ are not available in the studied area (see http://www-naweb.iaea.org/napc/ih/IHS_resources_gnip.html). Here, we tested the impact of using two different methods for deriving $\delta^{18}O_P$ time series.

First, a linear model was used to estimate the daily values of $\delta^{18}O_P$ and subsequently $\delta^{18}O_V$ based on the primary drivers of their temporal variability (Dansgaard, 1964; Horita and Wesolowski, 1994), that are air temperature (T_{air}; °C) and precipitation at the corresponding site (P; mm):

$$\delta^{18}O_P = a \cdot T_{air} + b \cdot P + c \quad (2)$$

$$\delta^{18}O_V = \delta^{18}O_P - \varepsilon^{*}_{Tair} \quad (3)$$

with ε^{*}_{Tair} the fractionation due to the change of phase from liquid water to vapour at the mean air temperature. The coefficients *a* and *b* were allowed to vary over a plausible range (or prior range) in the calibration process together with other MAIDENiso parameters, while coefficient *c* was

fixed to a likely value (see Table 1 and section 2.4). This estimated set of data is referred in the following as the estimated $\delta^{18}O_P$ dataset.

Second, we run the model with the series of the daily $\delta^{18}O_P$ derived from two general circulation models (GCM) with different spatial resolutions and enough available data at our site locations: 1) the MUGCM model (Noone and Simmonds, 2002) forced by varying sea surface temperature (SST) from the HadISST data set for the 1950-2003 period (2°×2° resolution; extracted at http://paos.colorado.edu/~dcn/SWING/database.php ; hereafter referred as MUGCM $\delta^{18}O_P$ dataset), and 2) the Laboratoire de Météorologie Dynamique Zoom (LMDZ5A) model (Hourdin et al., 2013; Risi et al., 2010) with the horizontal winds guided by those of the National Centers for Environmental Protection - 20th Century Reanalysis (NCEP20) for the 1950-2008 period (Compo et al., 2011) (2.5°×3.75° resolution; hereafter referred as LMDZ-NCEP20 $\delta^{18}O_P$ dataset).

The final $\delta^{18}O_{TR}$ time series are the annual average of the $\delta^{18}O_{TR}$ daily values (Eq. 1) weighted by the daily simulated stand Gross Primary Production (GPP), assuming a proportional allocation of carbon to the trunk. For the northeastern Canadian sites, the GPP simulated by MAIDENiso was optimized using observations from an eddy covariance station (see Gennaretti et al. (2017a)). Unfortunately, such observations were not available for *N. pumilio*, and therefore the parameterization obtained for the GPP of *P. mariana* was also used for the western Argentinian sites but constraining the simulations with phenological observations extracted from the literature. For example, to respect the annual cycle of the leaf area index (LAI) for *N. pumilio* (Magnin et al., 2014; Rusch, 1993), we used in MAIDENiso a seasonal LAI annual cycle with a development of leaves (LAI increase) between October and November, a maximum LAI (set at 5 leaf area/ground area) from November to April, a decreasing LAI (leaf fall) between April and May, and finally a leafless period (null LAI) from June to September (Magnin et al., 2014; Rusch, 1993). Furthermore, based on the finding that $\delta^{18}O_{TR}$ annual time series were more correlated to climate variables of specific months of the growing season (Lavergne et al., 2016), we also computed $\delta^{18}O_{TR}$ annual values by weighting the $\delta^{18}O_{TR}$ daily values (Eq. 1) with synthetic GPP time series maximizing the correspondence between observations and simulations.

2.3. Meteorological and atmospheric CO_2 data

At the western Argentinian sites, we did not have long daily records of observed climate data. Therefore, daily minimum–maximum temperature and precipitation data were derived from the 20th Century Reanalysis V2c (Compo et al., 2011) provided by the NOAA/OAR/ESRL (2°×2° resolution, https://www.esrl.noaa.gov/psd/data/gridded/data.20thC_ReanV2c.html), which is one of the few reanalysis products covering entirely the 20th century. The temperature daily time series of the reanalysis were corrected in order to respect the monthly mean values detected at Bariloche, the nearest meteorological station from our sampling sites (~48 km from the sites, 41°12′ S–71°12′ W, 840 m asl; Servicio Meteorológico Nacional, Argentina). The resulting maximum and minimum temperature series, covering the 1952-2011 period, fit well with the daily local temperature data from La Almohadilla (ALM) site (41°11'S, 71°47'W, 1410 m asl; data measured by dataloggers and provided by IANIGLA) available over the 2002-2012 period ($r = 0.74$, $p < 0.001$; Figure SM1). For the northeastern Canadian sites, climate data were obtained from the gridded interpolated Canadian database of daily minimum–maximum temperature and precipitation covering the 1950-2005 studied period (0.08°×0.08° resolution, (Hutchinson et al., 2009); http://cfs.nrcan.gc.ca/projects/3/4). In addition to these data we also used modelled daily data from the GCMs described above for both the western Argentinian and northeastern Canadian sites (see Table 2 with the input data used for each tested configuration).

Data on the atmospheric CO_2 concentration were derived from the Mauna Loa station over the 1958-2012 period (Keeling et al. (1976); http://www.esrl.noaa.gov/gmd/ccgg/trends/). For the years 1950-1957, we extrapolated atmospheric CO_2 data using the trend and seasonal cycle observed in the observations over the subsequent 10-years period (1958-1967).

2.4. Estimation of parameters influencing $\delta^{18}O_{TR}$

We used a Bayesian method for the simultaneous calibration of the various MAIDENiso parameters specific to the study species and site. A set of 50 plausible blocks of parameters (posterior values) was selected according to the method described in Gennaretti et al. (2017a) using Markov Chain Monte Carlo (MCMC) sampling (Table 1). The following prior plausible ranges were considered:

1) the prior ranges of the *a* and *b* coefficients in the equation of the daily $\delta^{18}O_P$ (Eq. 2) were selected in order to get $\delta^{18}O_P$ values for each site consistent with the measured monthly local

values from the nearest stations of the Global Network of Isotopes in Precipitation (GNIP), and with the simulated daily values from the LMDZ-NCEP20 model and from the MUGCM model (see Table 1),

2) the range for the biochemical fractionation factor ε_0 was chosen between 24‰ and 30‰ (+27±3‰ after DeNiro and Epstein (1981); Sternberg (1989); Yakir and DeNiro (1990)),

3) the range for the kinetic fractionation ε_k, which has been set to 26.5‰ in Farquhar et al. (1989) but that can vary over larger ranges (Buhay et al., 1996), was taken between 10‰ and 30‰ here,

4) the range for the dampening factor f_o was allowed to vary between 0.3 and 0.5 following Saurer et al. (1997).

We tested the sensitivity of the MAIDENiso model to the calibrated parameters by modifying them within their respective prior calibration range. To control the robustness of the calibrated parameters, we performed the calibration of these parameters over two equal length intervals (1950-1977 and 1978-2005 for *P. mariana*; 1952-1981 and 1982-2011 for *N. pumilio*) keeping the second half for independent validation of the parameters estimates. Once the model was calibrated for the two species, the MAIDENiso's performance to simulate *P. mariana* and *N. pumilio* $\delta^{18}O_{TR}$ interannual data was evaluated using the correlation coefficients (r) and the root mean square errors (RMSE) between observed and simulated values. This is a standard approach to evaluate how well a mechanistic model is simulating $\delta^{18}O_{TR}$ variations (e.g. Danis et al., 2012; Lorrey et al., 2016).

2.5. Disentangling leaf-level fractionation processes and source water influences on $\delta^{18}O_{TR}$ signature

To define the relative contributions to the $\delta^{18}O_{TR}$ signature of the isotopic signal of the source water (xylem water) and of the fractionation processes due to transpiration taking place in the leaves, we designed two experimental simulations with MAIDENiso based on Eq. 1:

1) to quantify the influence of the variability of the isotopic composition of the xylem water on $\delta^{18}O_{TR}$, we compared the reference simulations to those where the relative humidity (h_{air}) and the isotopic composition of atmospheric vapour ($\delta^{18}O_V$) were assumed to be constant. The constant values for h_{air} and $\delta^{18}O_V$ were defined as the averages of the respective MAIDENiso outputs (h_{air} = 0.62 and 0.9, and, $\delta^{18}O_V$ = -26.28‰ and -17.34‰,

respectively for northeastern Canada and western Argentina; the XW source experiment simulation hereafter),

2) to quantify the influence of the isotopic enrichment of the leaf water due to transpiration on $\delta^{18}O_{TR}$, we compared the reference simulations to those where the $\delta^{18}O_{XW}$ series were assumed to be constant. The constant value for $\delta^{18}O_{XW}$ was estimated as the average of the $\delta^{18}O_{XW}$ MAIDENiso outputs ($\delta^{18}O_{XW}$ = -13.81‰ and -7.03‰, respectively for northeastern Canada and western Argentina; the Leaf water enrichment driven experiment simulation hereafter).

Comparison between the experimental and reference simulations (i.e. using the optimal values of the parameters) was achieved through the calculation of the coefficient of determination (R^2).

3. RESULTS

3.1. Estimated versus modelled and observed $\delta^{18}O_P$ values

The modelled $\delta^{18}O_P$ series from the GCM models are similar to the GNIP datasets, with mean values ranging from -12‰ to -8‰ over June-September in northeastern Canada (Figure SM2A) and from -7‰ to -3‰ over December-April at the western Argentinian sites (Figure SM2B). In general, $\delta^{18}O_P$ series from LMDZ-NCEP20 model in western Argentina are slightly displaced toward higher values (+1‰) in comparison with the GNIP and MUGCM data. The estimated $\delta^{18}O_P$ values based on plausible values of coefficients *a* and *b* agree well with those of the models and observations in northeastern Canada. For the western Argentinian sites, they are 2-3‰ lower from April to October, i.e. late spring-early autumn (Figure SM2).

3.2. Sensitivity of the model to the calibrated parameters

Most of the calibrated parameters have an influence on the correlations between observed and simulated $\delta^{18}O_{TR}$ series and/or on the mean levels of the simulated series (Figure 2). The temperature and precipitation dependences of $\delta^{18}O_P$ values (respectively *a* and *b* coefficients) have the strongest influence on correlations. Increasing *a* and *b* values increase the mean $\delta^{18}O_{TR}$ levels, more strongly in western Argentina than in northeastern Canada (Figure 2). Changes in the dampening factor (f_o) and in the biochemical fractionation (ε_0) have almost no effect on correlation, but their increase induces significant decrease of the mean levels of $\delta^{18}O_{TR}$ series.

Finally, increasing the kinetic fractionation (ε_k) leads to lower correlations and to higher mean levels of $\delta^{18}O_{TR}$ (Figure 2).

3.3. MAIDENiso performance in reproducing observed $\delta^{18}O_{TR}$ series

Split-period verifications of the calibrated relationships for *P. mariana* and *N. pumilio* when using estimated $\delta^{18}O_P$ series from Eq. 2 indicate that the calibration over either the first half or the second half periods provide similar posterior densities of the calibrated parameters than the ones obtained when calibrating over the whole periods (Figure SM3). One exception is observed in the calibration of coefficient *a* in northeastern Canada over the two half periods, where the posterior densities of *a* are different from the one obtained by calibrating over the entire period. Over the entire periods, observed and simulated $\delta^{18}O_{TR}$ series are significantly correlated in northeastern Canada ($r = 0.56$, $p < 0.01$ and RMSE = 0.67; Figure 3A) and in western Argentina ($r = 0.48$, $p < 0.01$ and RMSE = 0.63; Figure 3C). The correlation between observed and simulated $\delta^{18}O_{TR}$ series are slightly improved when we used synthetic daily GPP ($r = 0.62$ and $r = 0.52$, $p < 0.01$, respectively for northeastern Canada and western Argentina; Figure 3B and 3D). It is worth noting that the mean levels of the simulated $\delta^{18}O_{TR}$ series for the Argentinian sites are lower than those of the observations (offset of around -2.5‰; Figure SM4). The series were therefore corrected to respect the mean values detected in the observations (Figure 3C and 3D). In contrast, the correlations between observation and simulation considerably decrease when we used modelled $\delta^{18}O_P$ from MUGCM models or LMDZ-NCEP20 reanalysis data. They only reach $r = 0.13$ ($p > 0.05$) to 0.23 ($p < 0.05$) in northeastern Canada and $r = 0.23$ to 0.26 ($p < 0.05$) in western Argentina, respectively (Figure 4).

3.4. Influence of source water and leaf water isotopic enrichment to the $\delta^{18}O_{TR}$ signature

The relative contributions to the $\delta^{18}O_{TR}$ signature of the isotopic signal of the source (xylem) water and of the ^{18}O enrichment of the leaf water due to transpiration were investigated. In both regions, the Leaf water enrichment experimental simulations are more highly related to the reference simulations (R^2 centred on 0.9 and 0.95, respectively for northeastern Canada and western Argentina; Figure 5) than are the XW source simulations (R^2 centred on 0.65 and 0.8, respectively for northeastern Canada and western Argentina). This suggests that, with the model, the variability of $\delta^{18}O_{XW}$ has a weaker influence on $\delta^{18}O_{TR}$ variations than the changes of the leaf

water isotopic enrichment do. Notably, *P. mariana* in northeastern Canada appears to be more sensitive to both influences than *N. pumilio* in western Argentina (Figure 5).

4. DISCUSSION

4.1. Precipitation $\delta^{18}O_P$ variations and estimation

Although the regression models used to predict daily $\delta^{18}O_P$ values are likely too simplistic, the resultant monthly averaged values adequately reproduce the distribution of the observed (from GNIP stations) and modelled (by GCMs) monthly $\delta^{18}O_P$ series in northeastern Canada. In western Argentina, the distribution of monthly $\delta^{18}O_P$ values is also well reproduced but the amplitude of variation of the predicted values is too high, leading to simulated values lower than the measured ones during the colder months. The temporal $\delta^{18}O_P$ variations are positively related to air temperature given the positive coefficient *a*. In agreement with the simple Rayleigh distillation model (Dansgaard, 1964), as air temperature decreases, the specific humidity at saturation decreases, and water vapour condenses. $H_2{}^{18}O$ condenses preferentially, the residual water vapour gets more and more depleted as condensation proceeds. Consequently, in the Tropics, the $^{18}O/^{16}O$ ratio in the meteoric water has been observed to decrease with increasing amount of precipitation and/or relative humidity (Rozanski et al., 1993). In extra-tropical regions, $\delta^{18}O_P$ may also correlate with precipitation amount (negative coefficient *b*), since both variables depend on the meteorological conditions.

The results of the linear regressions show comparatively lower influence of precipitation on $\delta^{18}O_P$ in western Argentina than in northeastern Canada (Table 1). This suggests that the imprint of the precipitation amount on $\delta^{18}O_P$ in western Argentina is low and that $\delta^{18}O_P$ variations are mainly controlled by seasonal changes in temperature, which is in agreement with previous work (Rozanski et al., 1995). However, due to the strong west-to-east precipitation gradient in this region (orographic rain shadow), large $\delta^{18}O_P$ variations occur over short distances (Rozanski et al., 1995; Smith and Evans, 2007; Stern and Blisniuk, 2002). Therefore, the daily precipitation dataset extracted from the gridded reanalysis data, which has a low spatial resolution (>200 km), may not represent the daily variations in precipitation at a local scale faithfully. Therefore, the model may underestimate the contribution of precipitation on $\delta^{18}O_P$ variability in this particular area.

In contrast, in northeast Canada, both temperature and precipitation amount equally control the $\delta^{18}O_P$ variations. The high amount of precipitation falling in summer (~46%) should have a strong effect and decrease the $\delta^{18}O_P$ values in the condensed water, while high temperatures counteract this effect by increasing this ratio. Before reaching northeastern Canada, the air masses pushed by the dominant westerly winds discharge most of their humidity over the land, leading to a depleted $\delta^{18}O_P$ signal at our sites (for the same reason, $\delta^{18}O_{TR}$ values at L20, which is located 110 km North-East of L01, are ~1‰ lower). Moreover, the $\delta^{18}O_P$ signal in the Canadian sites is comparatively more depleted than in the Argentinian sites, because of their higher latitude. It is worth noting that the resolution of the gridded meteorological dataset used for the Canadian sites is relatively high (~10 km), which means that the local processes are likely well represented.

4.2. Relative performance in modelling $\delta^{18}O_{TR}$ values

The simulated $\delta^{18}O_{TR}$ series based on daily $\delta^{18}O_P$ estimation from the regression models reproduce the observations better than the ones based on $\delta^{18}O_P$ values derived from GCMs (Figure 4). This is in part due to the greater number of parameters to optimize, as the calibration process can more easily find a solution that fits the observations better. This may however reflect error compensations especially in western Argentina where the estimated annual variability of $\delta^{18}O_P$ is too large. Conversely in northeastern Canada, the annual variations of $\delta^{18}O_P$ that are estimated, simulated by GCMs and observed are in good agreement (Figure SM2). Although isotope-enabled atmospheric global models can reproduce the mean annual precipitation isotopic values and seasonality for many areas (Risi et al., 2010), results at specific sites, especially in mountainous regions such as at our western Argentinian site, can be less accurate (Figure SM2; see the offset between GNIP stations and LMDZ-NCEP20). Ideally, daily $\delta^{18}O_P$ long-term records from meteorological stations in the study region should be used as an input of MAIDENiso. Simulations from high-resolution regional circulation models, such as REMOiso which has a 0.5°×0.5° (~55 km) horizontal resolution (Insel et al., 2013; Sturm et al., 2007, 2005), may produce reliable local $\delta^{18}O_P$ values. Such dataset has proven to be quite helpful with MAIDENiso in the Fontainebleau forest (France) (Danis et al., 2012). However, up to now, measured or REMOiso $\delta^{18}O_P$ datasets in our regions of study do not exist, which is the case for most regions of the world. Moreover, early data (1970-80s) from GNIP stations may have been

391 compromised by pan evaporation and therefore isotopic enrichment. Therefore, we recommend
392 that daily GNIP stations are set up in various forested ecosystems, that en effort is accomplished
393 to homogenize older GNIP time series, and that high resolution simulations of $\delta^{18}O_P$ are
394 performed in wider regions.
395
396 The modelling of $\delta^{18}O_{TR}$ values based on the estimation of $\delta^{18}O_P$ is relatively more accurate for
397 northeastern Canada than for western Argentina (Figure 3). As the mean levels of the measured
398 $\delta^{18}O_{TR}$ values are high at the western Argentinian sites (mean value of about 30‰), the Bayesian
399 optimization tends to increase the biochemical (ε_0) and kinetic (ε_k) fractionations as well as the
400 coefficient *a*, while reducing the dampening factor (f_o) to reach more representative mean levels
401 of the $\delta^{18}O_{TR}$ simulation. But still, these levels are too low in comparison with the observations
402 (about 2.5‰ lower; Figure SM4). When the posterior value of a calibrated parameter is limited to
403 the upper bound of the prior range of plausible values, as it is the case at the western Argentinian
404 sites for *a*, *b* and ε_0 (Figure SM3), it means that either the prior range is too narrow, or the model
405 is inadequate, or some important process is not considered in the model. Here, the estimation of
406 the prior ranges of both coefficients *a* and *b* were based on observed (GNIP stations) and
407 simulated (GCMs) $\delta^{18}O_P$ values. Therefore, we expect their respective ranges to be consistent
408 with local processes. When the prior range of *a* is extended to higher values in the optimization
409 process, observed and simulated $\delta^{18}O_{TR}$ mean levels in western Argentina are better matching.
410 However, in this case, the distribution of $\delta^{18}O_P$ values is shifted toward higher values, advocating
411 for unrealistic estimated $\delta^{18}O_P$ variations.
412 One other possibility is that the prior range of ε_0 is too narrow. In accordance with DeNiro and
413 Epstein (1981), Sternberg (1989) and Yakir and DeNiro (1990), the biochemical fractionation ε_0
414 is assumed here to be lower than 30‰. However, a recent study has demonstrated that this
415 parameter, nearly constant between 20 to 30°C, increases at lower temperatures to values of 31‰
416 (Sternberg and Ellsworth, 2011). During the growing season, maximum temperatures can reach
417 20°C in western Argentina and 30°C in northeastern Canada, which suggests that the high mean
418 $\delta^{18}O_{TR}$ levels in *N. pumilio* may be due to biochemical fractionation higher than 30‰ due to
419 temperature generally lower than 20°C. However, when the prior range of ε_0 is extended to 31‰
420 in the optimization process, the mean $\delta^{18}O_{TR}$ levels of *N. pumilio* are still too low in comparison
421 with the observations. These results advocate for the existence of other processes, which can

explain this offset in mean levels in Argentina. For example, higher soil water evaporation than modelled by MAIDENiso should lead to less negative $\delta^{18}O_{SW}$ (and therefore $\delta^{18}O_{XW}$), which could explain the high mean levels of $\delta^{18}O_{TR}$ in Argentina. Caution should be exercised with such an interpretation since other species living in similar conditions as *N. pumilio* in western Argentina show comparatively lower mean $\delta^{18}O_{TR}$ levels than *N. pumilio* (i.e., *Fitzroya cupressoides*; see Lavergne et al. (2016)). The ongoing monitoring and evaluation of isotopic processes based on synchronous measurements of vapour, precipitation, soil water and xylem water will certainly help understanding the high mean levels observed in Argentina, and increasing the representation of the involved processes in MAIDENiso.

The better fit between observed and simulated $\delta^{18}O_{TR}$ values obtained with specific forms of synthetic distributions of daily GPP for northeastern Canada and western Argentina (Figure 3) suggests differential limiting factors in the two regions. The synthetic bimodal distribution of daily GPP with maxima in spring and autumn, as simulated in western Argentina, is often observed in a diversity of ecosystems such as in the Mediterranean environments (Baldocchi et al., 2010; Gea-Izquierdo et al., 2015). After the activation of the photosynthesis in early spring, increasing temperatures tend to be optimal for tree growth. However, in a modelling study, Lavergne et al. (2015) have shown that the influence of temperature on *N. pumilio*'s growth becomes negative once a temperature threshold (soil moisture) is exceeded. Therefore, we assume that after reaching a threshold of temperature and soil moisture summer conditions, tree growth is inhibited, leading to a decrease of primary productivity. However, when temperature starts to decline and soil water supply tends to increase with increasing precipitation events, tree growth increases again until the end of the growing season. In contrast, because precipitation is more abundant in summer (June to September) in northeastern Canada (Naulier et al., 2014), high summer temperatures should be always beneficial to tree-growth if enough soil water is available. Therefore, in agreement with GPP-derived eddy covariance data from the Fluxnet network (see Gennaretti et al. (2017a)), a better fit between observations and simulations is observed when using a unimodal rather than a bimodal GPP distribution. Monitoring of tree physiology, environmental conditions and wood cell formation will provide a more detailed representation of the complex biological and ecological processes operating in Patagonia, allowing us to run the MAIDENiso model with better constraints.

4.3. What is the main origin of the temperature signal recorded in $\delta^{18}O_{TR}$?

The investigation of the relative contributions of the isotopic composition of the source (xylem) water and of the ^{18}O enrichment of the leaf water by transpiration on the simulated $\delta^{18}O_{TR}$ reveals that the variability of the former has a weaker influence on $\delta^{18}O_{TR}$ variations than that of the latter in North and South America. Therefore, the temperature signal recorded in $\delta^{18}O_{TR}$ series more likely reflects the effect of temperature on isotopic enrichment of the leaf water rather than on the isotopic composition of the source water. At the leaf-level, air temperature has a strong effect on the relative humidity and therefore on the vapour pressure deficit (VPD), i.e. the difference between the saturation vapour pressure and the actual vapour pressure, which modulates the transpiration (Barbour, 2007). Thus, the imprint of the ambient air temperature on the fractionation processes occurring during transpiration is preferentially recorded in the tree rings of the two species. Furthermore, both the isotopic signature of the xylem water and of the fractionation processes occurring at the evaporation sites of the leaves have comparatively higher influence on $\delta^{18}O_{TR}$ in *P. mariana* than in *N. pumilio*. This is probably due to the lower amplitude of the day-by-day variations of the relative humidity in western Argentina (SD = 5%) versus in northeastern Canada (SD = 16%) that translates into a weaker influence of h_{air} variations and therefore of leaf-level isotopic fractionation processes on $\delta^{18}O_{TR}$ values in western Argentina than in northeastern Canada. These results highlight the potential of MAIDENiso model to better refine the origin of the climatic signal recorded in the oxygen isotopic signature in the tree-rings of different species.

5. CONCLUSION

Here, by using MAIDENiso model, we provided a mechanistic overview of the climatic and biological processes controlling oxygen isotopic fractionation in two American temperature-sensitive tree species. First, we have shown that using regression-based rather than model-based $\delta^{18}O_P$ estimates as inputs increases the predictive skills of our simulations, although this may be at the price of error compensations. Second, our study reveals that the variability of the isotopic composition of the source (xylem) water has a weaker influence on $\delta^{18}O_{TR}$ variations than that of the ^{18}O enrichment of the leaf water by transpiration. Last, these findings suggest that the imprint

of temperature recorded in $\delta^{18}O_{TR}$ of the two species is likely related to the effect of temperature on isotopic enrichment of the leaf water. The isotopic monitoring of water within the soil-vegetation-atmosphere compartments in future work will certainly provide the input and control data necessary to better constrain MAIDENiso. Our study demonstrates that the eco-physiological modelling of $\delta^{18}O_{TR}$ values is necessary and likely the only approach to accurately interpret the recorded climate signal. Based on the calibrations of MAIDENiso presented here, the next step involves inverse modelling approaches to perform paleoclimatic reconstructions in North and South America that are less biased by the complex and nonlinear interactions between climate, CO_2 concentrations and tree growth as recommended by Boucher et al. (2014).

ACKNOWLEDGMENTS

A.L. has been supported by a Research associate/Lecturer position at the Aix-Marseille University (France). F.G. has received funding from the European Union's Horizon 2020 research and innovation program under the Marie Sklodowska-Curie grant agreement No 656896. We acknowledge all data providers: the Instituto Argentino de Nivología, Glaciología y Ciencias Ambientales (IANIGLA, Argentina) for providing the daily temperature data from La Almohadilla site; the National Meteorological Service from Argentina for providing the monthly temperature data from Bariloche meteorological station (Argentina); the Department of Natural Resources Canada for providing the daily climatic data used for Quebec; the US Department of Energy, Office of Science Biological and Environmental Research (BER) and the National Oceanic and Atmospheric Administration Climate Program Office for providing the daily climatic data used for Argentina; and the SWING project for providing the daily $\delta^{18}O_P$ data from MUGCM model.

References

Baldocchi, D. D., Ma, S., Rambal, S., Misson, L., Ourcival, J. M., Limousin, J. M., Pereira, J. and Papale, D.: On the differential advantages of evergreenness and deciduousness in mediterranean oak woodlands: A flux perspective, Ecol. Appl., 20(6), 1583–1597, doi:10.1890/08-2047.1, 2010.

Barbour, M. M.: Stable oxygen isotope composition of plant tissue: a review, Funct. Plant Biol., 34, 83–94, doi:10.1071/FP06228, 2007.

Barbour, M. M., Cernusak, L. A. and Farquhar, G. D.: Factors affecting the oxygen isotope ratio

514 of plant organic material, in Stable isotopes and biosphere-atmosphere interactions: Processes
515 and Biological Controls, edited by L. B. Flanagan, J. R. Ehleringer, and D. E. Pataki, pp. 9–28,
516 Elsevier, Amsterdam., 2005.
517 Boucher, E., Guiot, J., Hatté, C., Daux, V., Danis, P. A. and Dussouillez, P.: An inverse modeling
518 approach for tree-ring-based climate reconstructions under changing atmospheric CO_2
519 concentrations, Biogeosciences, 11(12), 3245–3258, 2014.
520 Brienen, R. J. W., Helle, G., Pons, T. L., Guyot, J.-L. and Gloor, M.: Oxygen isotopes in tree
521 rings are a good proxy for Amazon precipitation and El Niño-Southern Oscillation variability,
522 Proc. Natl. Acad. Sci., 109(42), 16957–16962, doi:10.1073/pnas.1205977109, 2012.
523 Buhay, W. M., Edwards, T. W. D. and Aravena, R.: Evaluating kinetic fractionation factors used
524 for reconstructions from oxgen and hydrogen isotope ratios in plant water and cellulose,
525 Geochemistry, Geophys. Geosystems, 60(12), 2209–2218, 1996.
526 Cernusak, L. A. and English, N. B.: Beyond tree-ring widths: stable isotopes sharpen the focus on
527 climate responses of temperate forest trees, Tree Physiol., 35(1), 1–3,
528 doi:10.1093/treephys/tpu115, 2015.
529 Compo, G. P., Whitaker, J. S., Sardeshmukh, P. D., Matsui, N., Allan, R. J., Yin, X., Gleason, B.
530 E., Vose, R. S., Rutledge, G., Bessemoulin, P., BroNnimann, S., Brunet, M., Crouthamel, R. I.,
531 Grant, A. N., Groisman, P. Y., Jones, P. D., Kruk, M. C., Kruger, A. C., Marshall, G. J., Maugeri,
532 M., Mok, H. Y., Nordli, O., Ross, T. F., Trigo, R. M., Wang, X. L., Woodruff, S. D. and Worley,
533 S. J.: The twentieth century reanalysis project, Q. J. R. Meteorol. Soc., 137(654), 1–28,
534 doi:10.1002/qj.776, 2011.
535 Craig, H. and Gordon, L. I.: Deuterium and oxygen 18 variations in the ocean and the marine
536 atmosphere, Spoleto, 1965.
537 Danis, P. A., Hatté, C., Misson, L. and Guiot, J.: MAIDENiso: a multiproxy biophysical model of
538 tree-ring width and oxygen and carbon isotopes, Can. J. For. Res., 42(9), 1697–1713,
539 doi:10.1139/x2012-089, 2012.
540 Danis, P. A., Masson-Delmotte, V., Stievenard, M., Guillemin, M. T., Daux, V., Naveau, P. and
541 von Grafenstein, U.: Reconstruction of past precipitation $\delta^{18}O$ using tree-ring cellulose $\delta^{18}O$ and
542 $\delta^{13}C$: A calibration study near Lac d'Annecy, France, Earth Planet. Sci. Lett., 243(3–4), 439–448,
543 doi:10.1016/j.epsl.2006.01.023, 2006.
544 Dansgaard, W.: Stable isotopes in precipitation, Tellus A, 16(4), 436–468,

545 doi:10.3402/tellusa.v16i4.8993, 1964.
546 DeNiro, M. J. and Epstein, S.: Relationship between the oxygen isotope ratios of terrestrial plant
547 cellulose, carbon dioside, and water, Science, 204, 51-53, 1979.
548 DeNiro, M. J. and Epstein, S.: Isotopic composition of cellulose from aquatic organisms,
549 Geochim. Cosmochim. Acta, 45(10), 1885–1894, doi:10.1016/0016-7037(81)90018-1, 1981.
550 Donoso, C.: Tipos forestales de los bosques nativos de Chile., Documento de Trabajo Nu. 38.
551 Investigación y Desarrollo Forestal (CONAF, PNUD-FAO). FAO Chile., 1981.
552 Farquhar, G. D., Barbour, M. M. and Henry, B. K.: Interpretation of oxygen isotope composition
553 of leaf material, in Stable isotopes: integration of biological, ecological and geochemical
554 processes, pp. 27–61, BIOS Scientific Publishers: Oxford., 1998.
555 Farquhar, G. D., Hubick, H. T., Condon, A. G. and Richards, R. A.: Carbon isotope fractionation
556 and plant water-use efficiency, in Stable isotopes in ecological research, pp. 21–40., 1989.
557 Gea-Izquierdo, G., Guibal, F., Joffre, R., Ourcival, J. M., Simioni, G. and Guiot, J.: Modelling
558 the climatic drivers determining photosynthesis and carbon allocation in evergreen Mediterranean
559 forests using multiproxy long time series, Biogeosciences, 12(12), 3695–3712, doi:10.5194/bg-
560 12-3695-2015, 2015.
561 Gennaretti, F., Arseneault, D., Nicault, A., Perreault, L. and Bégin, Y.: Volcano-induced regime
562 shifts in millennial tree-ring chronologies from northeastern North America., Proc. Natl. Acad.
563 Sci. U. S. A., 111(28), 10077-10082, doi:10.1073/pnas.1324220111, 2014.
564 Gennaretti, F., Gea-Izquierdo, G., Boucher, E., Berninger, F., Arseneault, D. and Guiot, J.:
565 Ecophysiological modeling of the climate imprint on photosynthesis and carbon allocation to the
566 tree stem in the North American boreal forest, Biogeosciences Discuss., in review,
567 doi:10.5194/bg-2017-51, 2017a.
568 Gennaretti, F., Huard, D., Naulier, M., Savard, M., Bégin, C., Arseneault, D. and Guiot, J.:
569 Bayesian multiproxy temperature reconstruction with black spruce ring widths and stable
570 isotopes from the northern Quebec taiga, Clim. Dyn., 1–13, doi:10.1007/s00382-017-3565-5,
571 2017b.
572 Gessler, A., Ferrio, J. P., Hommel, R., Treydte, K., Werner, R. A. and Monson, R. K.: Stable
573 isotopes in tree rings: towards a mechanistic understanding of isotope fractionation and mixing
574 processes from the leaves to the wood., Tree Physiol., 0, 1–23, 2014.
575 Guiot, J., Boucher, E. and Gea-Izquierdo, G.: Process models and model-data fusion in

dendroecology, Front. Ecol. Evol., 2, 52, doi:10.3389/fevo.2014.00052, 2014.
Hartl-Meier, C., Zang, C., Büntgen, U. L. F., Esper, J. A. N., Rothe, A., Göttlein, A., Dirnböck, T. and Treydte, K.: Uniform climate sensitivity in tree-ring stable isotopes across species and sites in a mid-latitude temperate forest., Tree Physiol., 2003(1), 4–15, doi:10.1093/treephys/tpu096, 2014.
Helliker, B. R. and Richter, S. L.: Subtropical to boreal convergence of tree-leaf temperatures, Nature, 454(7203), 511–514, doi:10.1038/nature07031, 2008.
Horita, J. and Wesolowski, D. J.: Liquid-vapor fractionation of oxygen and hydrogen isotopes of water from the freezing to the critical temperature, Geochim. Cosmochim. Acta, 58(16), 3425–3437, doi:10.1016/0016-7037(94)90096-5, 1994.
Hourdin, F., Grandpeix, J. Y., Rio, C., Bony, S., Jam, A., Cheruy, F., Rochetin, N., Fairhead, L., Idelkadi, A., Musat, I., Dufresne, J. L., Lahellec, A., Lefebvre, M. P. and Roehrig, R.: LMDZ5B: The atmospheric component of the IPSL climate model with revisited parameterizations for clouds and convection, Clim. Dyn., 40(9–10), 2193–2222, doi:10.1007/s00382-012-1343-y, 2013.
Hutchinson, M. F., McKenney, D. W., Lawrence, K., Pedlar, J. H., Hopkinson, R. F., Milewska, E. and Papadopol, P.: Development and testing of Canada-wide interpolated spatial models of daily minimum-maximum temperature and precipitation for 1961-2003, J. Appl. Meteorol. Climatol., 48(4), 725–741, doi:10.1175/2008JAMC1979.1, 2009.
Insel, N., Poulsen, C. J., Sturm, C. and Ehlers, T. A.: Climate controls on Andean precipitation $\delta^{18}O$ interannual variability, J. Geophys. Res. Atmos., 118(17), 9721–9742, doi:10.1002/jgrd.50619, 2013.
Kahmen, A., Sachse, D., Arndt, S. K., Tu, K. P., Farrington, H., Vitousek, P. M. and Dawson, T. E.: Cellulose $\delta^{18}O$ is an index of leaf-to-air vapor pressure difference (VPD) in tropical plants., Proc. Natl. Acad. Sci. U. S. A., 108(5), 1981–1986, doi:10.1073/pnas.1018906108, 2011.
Keeling, C. D., Bacastow, R. B., Bainbridge, A. E., Ekdahl Jr., C. A., Guenther, P. R., Waterman, L. S. and Chin, J. F. S.: Atmospheric carbon dioxide variations at Mauna Loa Observatory, Hawaii, Tellus A, 28, 538–551, doi:10.3402/tellusa.v28i6.11322, 1976.
Labuhn, I., Daux, V., Girardclos, O., Stievenard, M., Pierre, M. and Masson-Delmotte, V.: French summer droughts since 1326 AD: a reconstruction based on tree ring cellulose $\delta^{18}O$, Clim. Past, 11(6), 5113–5155, doi:10.5194/cpd-11-5113-2015, 2016.

Lavergne, A., Daux, V., Villalba, R. and Barichivich, J.: Temporal changes in climatic limitation of tree-growth at upper treeline forests: Contrasted responses along the west-to-east humidity gradient in Northern Patagonia, Dendrochronologia, 36, 49–59, 2015.

Lavergne, A., Daux, V., Villalba, R., Pierre, M., Stievenard, M. and Srur, A. M.: Improvement of isotope-based climate reconstructions in Patagonia through a better understanding of climate influences on isotopic fractionation in tree rings, Earth Planet. Sci. Lett., 459, 372–380, doi:10.1016/j.epsl.2016.11.045, 2017.

Lavergne, A., Daux, V., Villalba, R., Pierre, M., Stievenard, M., Srur, A. M. and Vimeux, F.: Are the $\delta^{18}O$ of F. cupressoides and N. pumilio promising proxies for climate reconstructions in northern Patagonia?, J. Geophys. Res. - Biogeosciences, 121(3), 767–776, doi:10.1002/2015JG003260, 2016.

López Bernal, P., Defossé, G. E., Quinteros, C. P. and Bava, J. O.: Sustainable management of lenga (Nothofagus pumilio) forests through group selection system, in Sustainable forest management - current research, edited by D. J. J. D. (Ed.), pp. 45–66, 2012.

Lorrey, A. M., Brookman, T. H., Evans, M. N., Fauchereau, N.C., Barbour, M., Macinnis-Ng, C. Criscitiello, A., Eischeid, G., Fowler, A. M., Horton, T. W. and Schrag, D. P.: Stable oxygen isotope signatures of early season wood in New Zealand kauri (Agathis australis) tree rings: Prospects for palaeoclimate reconstruction., Dendrochronologia, 40, 50–63, doi: 10.1016/j.dendro.2016.03.012, 2016.

Magnin, A., Puntieri, J. and Villalba, R.: Interannual variations in primary and secondary growth of Nothofagus pumilio and their relationships with climate, Trees, 28(5), 1463–1471, 2014.

Misson, L.: MAIDEN: a model for analyzing ecosystem processes in dendroecology, Can. J. For. Res., 34, 874–887, 2004.

Naulier, M., Savard, M. M., Bégin, C., Gennaretti, F., Arseneault, D., Marion, J., Nicault, A. and Bégin, Y.: A millennial summer temperature reconstruction for northeastern Canada using oxygen isotopes in subfossil trees, Clim. Past, 11(9), 1153–1164, doi:10.5194/cp-11-1153-2015, 2015.

Naulier, M., Savard, M. M., Bégin, C., Marion, J., Arseneault, D. and Bégin, Y.: Carbon and oxygen isotopes of lakeshore black spruce trees in northeastern Canada as proxies for climatic reconstruction, Chem. Geol., 374–375, 37–43, doi:10.1016/j.chemgeo.2014.02.031, 2014.

Noone, D. and Simmonds, I.: Associations between $\delta^{18}O$ of water and climate parameters in a

638 simulation of atmospheric circulation for 1979–95, J. Clim., 15, 3150–3169, 2002.
639 Ogée, J., Barbour, M. M., Wingate, L., Bert, D., Bosc, A., Stievenard, M., Lambrot, C., Pierre,
640 M., Bariac, T., Loustau, D. and Dewar, R. C.: A single-substrate model to interpret intra-annual
641 stable isotope signals in tree-ring cellulose, Plant, Cell Environ., 32(8), 1071–1090,
642 doi:10.1111/j.1365-3040.2009.01989.x, 2009.
643 Ogée, J., Brunet, Y., Loustau, D., Berbigier, P. and Delzon, S.: MuSICA, a CO_2, water and
644 energy multilayer, multileaf pine forest model: Evaluation from hourly to yearly time scales and
645 sensitivity analysis, Glob. Chang. Biol., 9(5), 697–717, doi:10.1046/j.1365-2486.2003.00628.x,
646 2003.
647 Rinne, K. T., Loader, N. J., Switsur, V. R. and Waterhouse, J. S.: 400-year May-August
648 precipitation reconstruction for Southern England using oxygen isotopes in tree rings, Quat. Sci.
649 Rev., 60, 13–25, doi:10.1016/j.quascirev.2012.10.048, 2013.
650 Risi, C., Bony, S., Vimeux, F. and Jouzel, J.: Water-stable isotopes in the LMDZ4 general
651 circulation model: Model evaluation for present-day and past climates and applications to
652 climatic interpretations of tropical isotopic records, J. Geophys. Res. Atmos., 115(12), 1–27,
653 doi:10.1029/2009JD013255, 2010.
654 Roden, J. S., Lin, G. and Ehleringer, J. R.: A mechanistic model for interpretation of hydrogen
655 and oxygen isotope ratios in tree-ring cellulose, Geochim. Cosmochim. Acta, 64(1), 21–35,
656 doi:10.1016/S0016-7037(99)00195-7, 2000.
657 Rozanski, K., Araguás-Araguás, L.: Spatial and temporal variability of stable isotope
658 composition of precipitation over the South American continent, Bull. l'Institut Fr. d'études
659 Andin., 24(3), 379–390, 1995.
660 Rozanski, K., Araguás-Araguás, L. and Gonfiantini, R.: Isotopic patterns in modern global
661 precipitation, in Climate change in continental isotopic records., edited by P. K. Swart, K. C.
662 Lohmann, J. McKenzie, and S. Savin, American Geophysical Union., 1993.
663 Running, S. W., Nemani, R. R. and Hungerford, R. D.: Extrapolation of synoptic meteorological
664 data in mountainous terrain and its use for simulating forest evapotranspiration and
665 photosynthesis, Can. J. For. Res., 17, 472–483, doi:10.1139/x87-081, 1987.
666 Rusch, V. E.: Altitudinal variation in the phenology of Nothofagus pumilio in Argentina, Rev.
667 Chil. Hist. Nat., 66(2), 131–141, 1993.
668 Saurer, M., Aellen, K. and Siegwolf, R. T. W.: Correlating $\delta^{13}C$ and $\delta^{18}O$ in cellulose of trees,

669 Plant, Cell Environ., 20, 1543–1550, 1997.
670 Saurer, M., Cherubini, P., Reynolds-Henne, C. E., Treydte, K. S., Anderson, W. T. and Siegwolf,
671 R. T. W.: An investigation of the common signal in tree ring stable isotope chronologies at
672 temperate sites, J. Geophys. Res. Biogeosciences, 113(4), doi:10.1029/2008JG000689, 2008.
673 Schlatter, J.: Requerimientos de sitio para la lenga, Nothofagus pumilio (Poepp. et Endl.) Krasser,
674 Bosque, 15, 3–10, 1994.
675 Shi, C., Daux, V., Zhang, Q. B., Risi, C., Hou, S. G., Stievenard, M., Pierre, M., Li, Z. and
676 Masson-Delmotte, V.: Reconstruction of southeast Tibetan Plateau summer climate using tree
677 ring $\delta^{18}O$: Moisture variability over the past two centuries, Clim. Past, 8(1), 205–213,
678 doi:10.5194/cp-8-205-2012, 2012.
679 Smith, R. B. and Evans, J. P.: Orographic precipitation and water vapor fractionation over the
680 Southern Andes, J. Hydrometeorol., 8(1), 3–19, doi:10.1175/JHM555.1, 2007.
681 Stern, L. A. and Blisniuk, P. M.: Stable isotope composition of precipitation across the southern
682 Patagonian Andes, J. Geophys. Res. Atmos., 107(23), doi:10.1029/2002JD002509p, 2002.
683 Sternberg, L. D. S. L.: Oxygen and hydrogen isotope ratios in plant cellulose: Mechanisms and
684 applications, in Stable isotopes in ecological research, edited by J. R. E. and K. A. N. P. W.
685 Rundel, pp. 124–141., 1989.
686 Sternberg, L. D. S. L. and Ellsworth, P. F. V.: Divergent biochemical fractionation, not
687 convergent temperature, explains cellulose oxygen isotope enrichment across latitudes, PLoS
688 One, 6(11), e28040, doi:10.1371/journal.pone.0028040, 2011.
689 Sturm, C., Vimeux, F. and Krinner, G.: Intraseasonal variability in South America recorded in
690 stable water isotopes, J. Geophys. Res. Atmos., 112(20), doi:10.1029/2006JD008298, 2007.
691 Sturm, K., Hoffmann, G., Langmann, B. and Stichler, W.: Simulation of $\delta^{18}O$ in precipitation by
692 the regional circulation model REMOiso, Hydrol. Process., 19(17), 3425–3444,
693 doi:10.1002/hyp.5979, 2005.
694 Treydte, K., Boda, S., Graf Pannatier, E., Fonti, P., Frank, D., Ullrich, B., Saurer, M., Siegwolf,
695 R. T. W., Battipaglia, G., Werner, W. and Gessler, A.: Seasonal transfer of oxygen isotopes from
696 precipitation and soil to the tree ring: Source water versus needle water enrichment, New Phytol.,
697 202(3), 772–783, doi:10.1111/nph.12741, 2014.
698 Viereck, L. A. and Johnston, W. F.: Picea mariana (Mill.) B. S. P., in Silvics of North America:
699 1. Conifers; 2. Hardwoods., edited by R. M. Burns and B. H. Honkala, pp. 443–464, US.

Department of Agriculture, Forest Service, Washington, DC., 1990.
Wernicke, J., Grießinger, J., Hochreuther, P. and Braüning, A.: Variability of summer humidity during the past 800 years on the eastern Tibetan Plateau inferred from $\delta^{18}O$ of tree-ring cellulose., Clim. Past, 11, 327–337, doi:10.5194/cp-11-327-2015, 2015.
Wershaw, R. L., Friedman, I. and Heller, S. J.: Hydrogen isotope fractionation in water passing through trees, in Advances in Organic Geochemistry, edited by F. Hobson and M. Speers, pp. 55–67, New York, Pergamon., 1966.
Yakir, D. and DeNiro, M. J.: Oxygen and hydrogen isotope fractionation during cellulose metabolism in lemna gibba L., Plant Physiol., 93(1), 325–332, doi:10.1104/pp.93.1.325, 1990.

Tables and Figures

Table 1 Definition of sensitive parameters. The posterior medians and 90% confidence intervals are also shown.

Parameter	Definition	Unit	Parameter type (prior range)	Values with 90% posterior confidence intervals
f_o	Dampening factor	NA	Calibrated (0.3 to 0.5)	0.36 [0.31; 0.46] (Arg.) 0.41 [0.32; 0.48] (Q.)
ε_0	Biochemical fractionation	‰	Calibrated (24 to 30)	29.99 [29.93; 30] (Arg.) 26.81 [24.74; 28.04] (Q.)
ε_k	Kinetic fractionation	‰	Calibrated (10 to 30)	28.86 [18.25; 29.96] (Arg.) 17.20 [11.16; 26.34] (Q.)
a	Temperature dependence of $\delta^{18}O_P$	NA	Calibrated (0.2 to 0.5 for Arg. and 0 to 0.38 for Q.)	0.50 [0.49; 0.50] (Arg.) 0.31 [0.25; 0.37] (Q.)
b	Precipitation dependence of $\delta^{18}O_P$	NA	Calibrated (-0.3 to 0 for Arg. and -0.39 to 0 for Q.)	-0.009 [-0.15; 0] (Arg.) -0.22 [-0.35; -0.14] (Q.)
c	Intercept of $\delta^{18}O_P$	‰	Fixed	-10.0 (Arg.) -11.9 (Q.)

719 **Table 2** Climate input data for all tested simulations
720

	Daily Tmin and Tmax	Daily P	Daily $\delta^{18}O_P$	CO_2
Configuration 1	Canadian database/ NOAA-CIRES dataset		Linear regression	Mauna Loa station
Configuration 2	Canadian database / NOAA-CIRES dataset	MUGCM data		
Configuration 3	LMDZ-NCEP20 data			

721
722

Figure 1 Tree-ring $\delta^{18}O$ time series (‰) at the three sites in Argentina (NUB, ALM and CHA in dark grey) and two sites in Quebec (L01 and L20 in dark grey; single trees in light grey). The bold black lines are the averaged values. The mean inter-site correlation coefficients are $r = 0.60$, $p < 0.05$ and $r = 0.80$, $p < 0.01$in the South and North American sites, respectively.

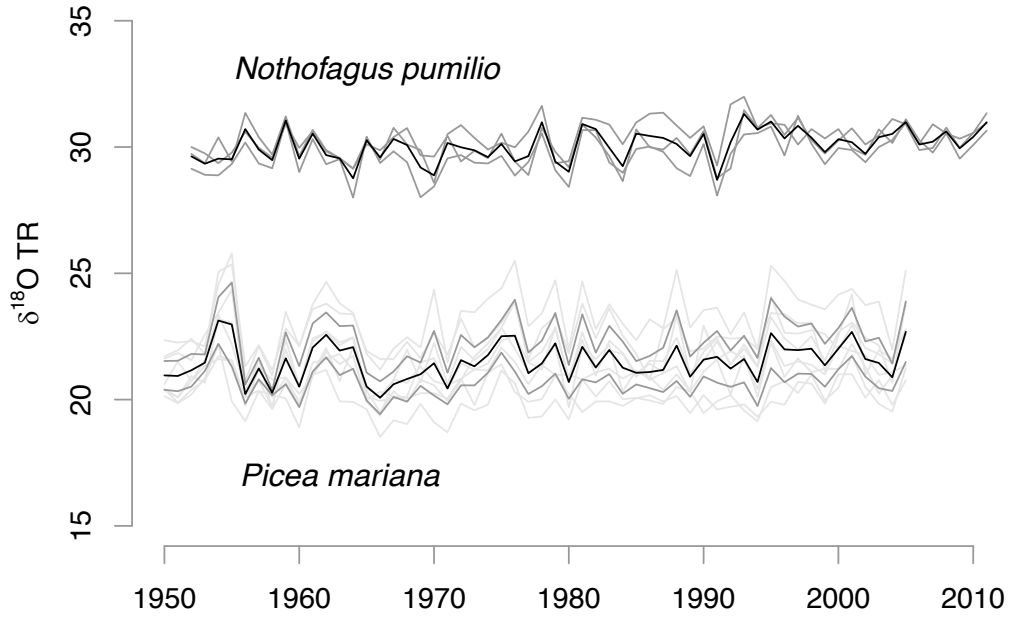

Figure 2 Dependence of the correlation coefficients between observed and simulated $\delta^{18}O_{TR}$ series (panels A), and of the mean simulated $\delta^{18}O_{TR}$ levels (‰) (panels B) as a function of the range of calibrated parameters *a*, *b*, f_o, ε_0 and ε_k for the 50 simulations performed. In black are the tests with the sites from Quebec and in red the oneswith the Argentinean sites. The vertical lines are the values of a plausible block of parameters retained in the MCMC optimization. The horizontal dashed lines are their respective 90% confidence interval calculated with 50 simulations (see Table 1). The horizontal dot lines in panel B are the mean values of the observed $\delta^{18}O_{TR}$.

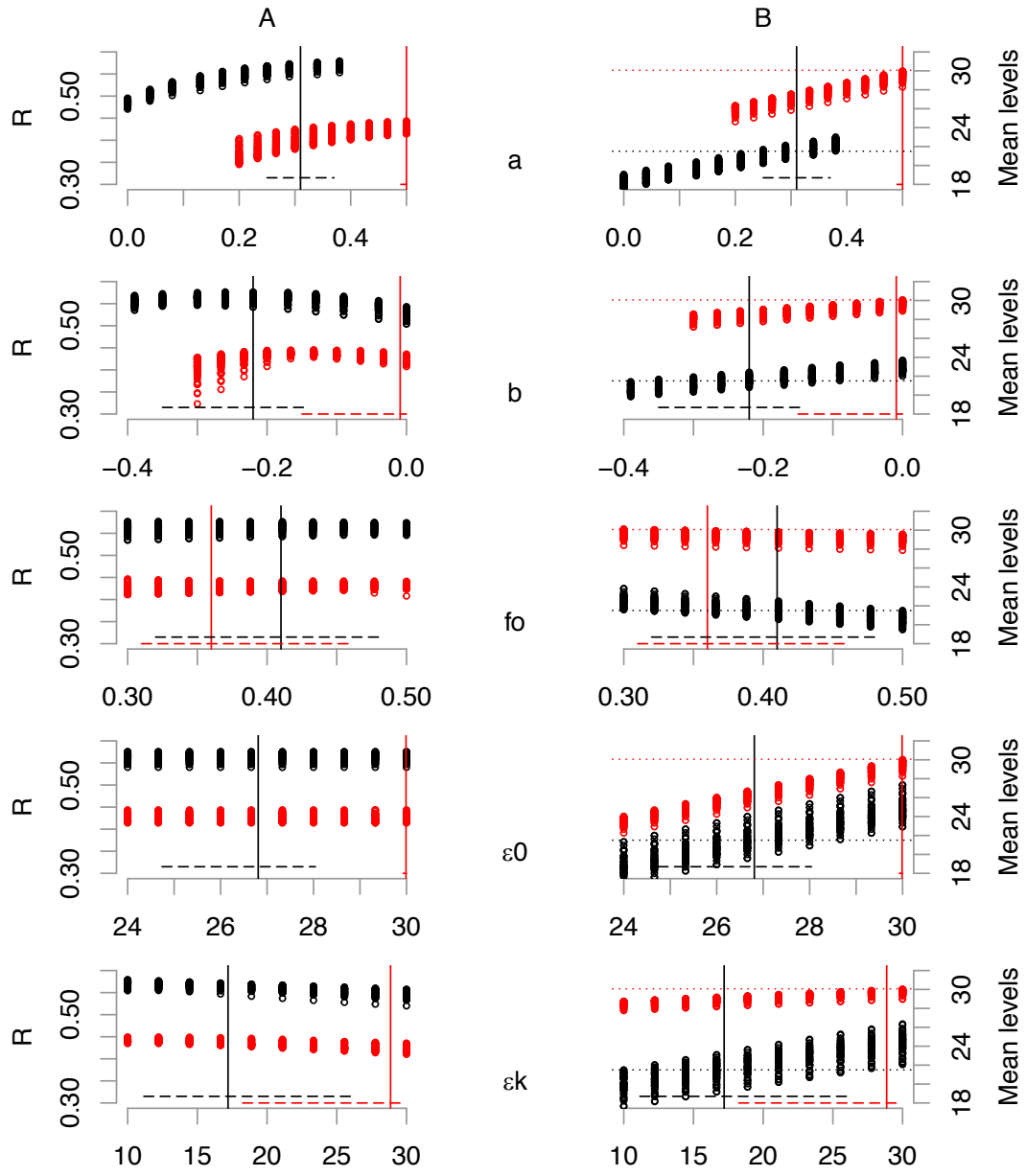

Figure 3 Comparison between observed (red or green) and simulated (grey) $\delta^{18}O_{TR}$ chronologies in Quebec (A and B) and Argentina (C and D), respectively, using GPP (in $gC.m^{-2}.day^{-1}$) simulated by MAIDENiso (A and C) or synthetized for maximizing correlations (B and D). The simulations are based on estimated $\delta^{18}O_P$ series. The 50 different simulations inferred from the Markov Chain Monte Carlo (MCMC) chains are in dark grey. The ± 1 root mean square error (RMSE) range is represented in light grey. The mean correlation coefficients are significant at 99% level (**).

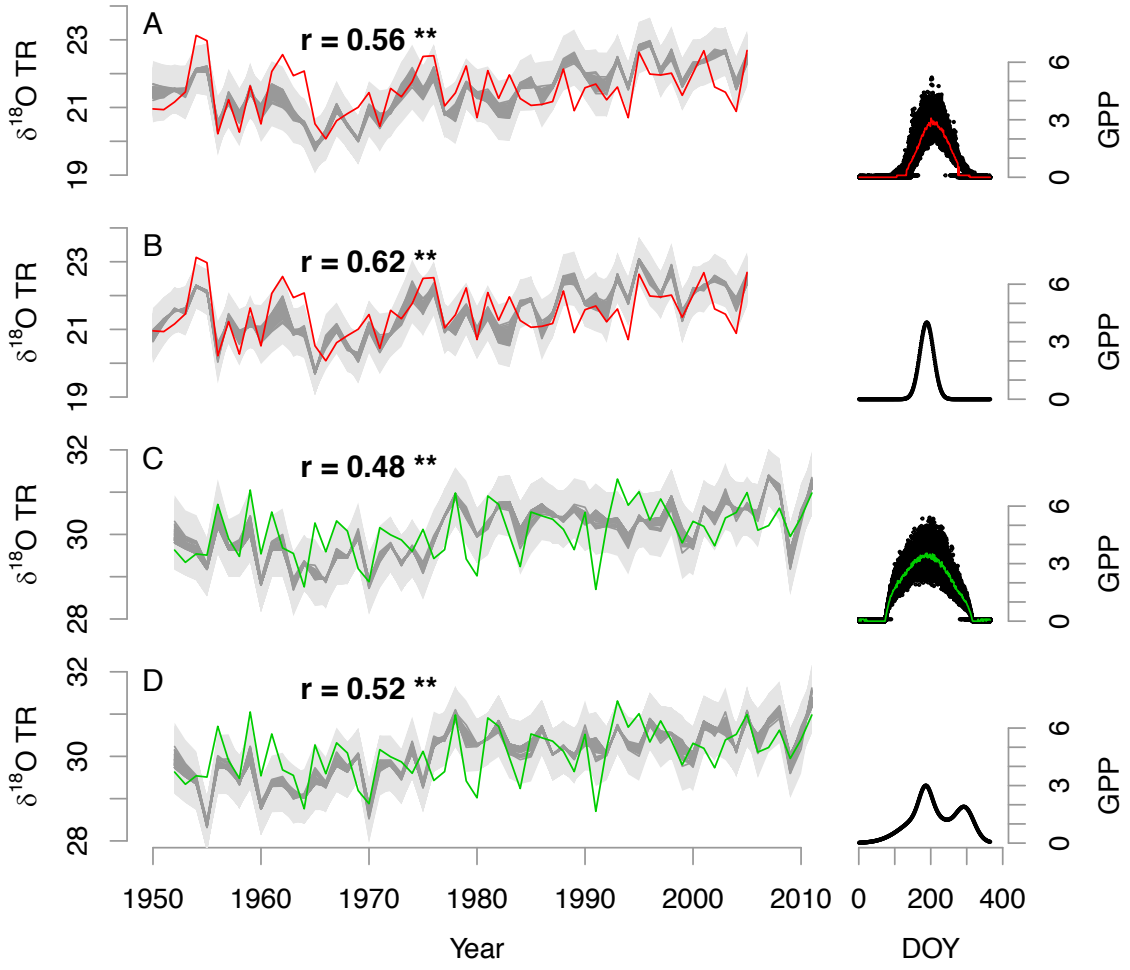

748 **Figure 4** Comparison of the densities of probability of the coefficient of correlation (R) between
749 observed and simulated $\delta^{18}O_{TR}$ chronologies in Quebec and Argentina when the simulations are
750 based on $\delta^{18}O_P$ series estimated by the regression model or from the MUGCM and LMDZ-
751 NCEP20 models.
752

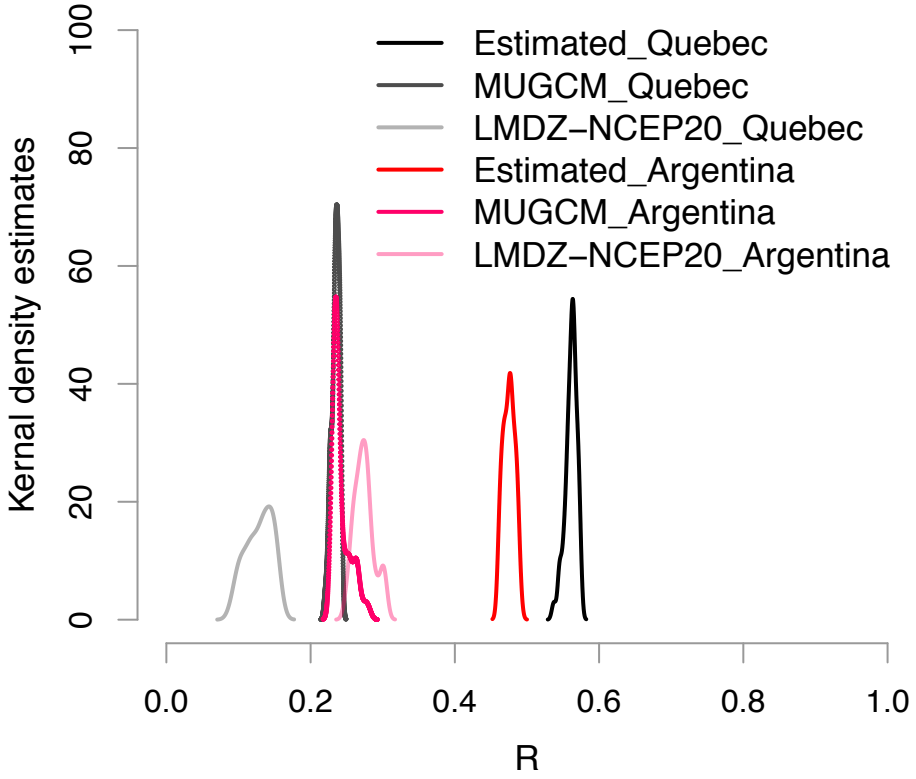

753
754

Figure 5 Density distributions of the coefficients of determination (R^2) between the reference simulations and the: 1) XW source experiment simulation ($\delta^{18}O_V$ and h_{air} set as constant, black) and, 2) Leaf water enrichment driven experiment simulation ($\delta^{18}O_{XW}$ set as constant, green) in Quebec (bold line) and Argentina (dashed line).